nature communications

Article

https://doi.org/10.1038/s41467-025-57989-y

Mechanically weak and highly dynamic state of mechanosensitive titin Ig domains induced by proline isomerization

Received: 11 September 2024

Accepted: 7 March 2025

Published online: 20 March 2025

Check for updates

Yukai Wang[1,2], Jiaqing Ye[1], Xian Liu[2], Zhuwei Zhang[1], Fei Shang[1,3], Xingyu Qi[1], Yuhang Zhang[1], Jingyi Du[2], Hao Sun[1,4], Jiashu Xu[1], Hu Chen[1,4] ✉, Miao Yu[2] ✉ & Shimin Le[1] ✉

Titin, essential for mechano-homeostasis in cardiac and skeletal sarcomere, contains numerous mechanosensitive immunoglobulin-like (Ig) domains in its I-band region. However, how proline isomerization and cysteine-mediated disulfide bond collectively regulate Ig domain dynamics within the physiological force range remains unclear. Here, we use single-molecule force spectroscopy to quantify the proximal Ig1 domain, revealing that proline isomerization leads to two native states–trans and cis states–with distinct mechanical and thermal stabilities. The trans-Ig1 unfolds at forces of ~ 5 pN, which is over 50 pN lower than that of cis-Ig1, and unfolds 1000 times faster under physiological forces. Furthermore, such proline induced dual-state is likely shared feature across majority of I-band Ig domains. Additionally, reduced cis- and trans-Ig1 exhibit catch-slip bond unfolding, while oxidized forms display slip-catch-slip unfolding. This study offers insight into effective modulation of proline isomerization and disulfide bond in regulating mechanosensitive proteins within the physiological force range.

In both cardiac and skeletal muscle, the giant force-transmitting protein titin forms a crucial connection between the Z-disk and the M-line within the sarcomere[1,2]. The tension-bearing I-band region of titin contains numerous immunoglobulin (Ig) domain repeats, with skeletal muscle titin having over 90 repeats and cardiac muscle titin containing more than 40 repeats[3]. These repeats are complemented by unstructured regions such as PEVK, N2A, and N2B[4–6]. Titin acts as a molecular spring, absorbing tension during sarcomere contraction-relaxation cycles and defining the passive elasticity of muscle[5,7–9]. This function relies on the elastic extension of the unstructured regions[4,5,10] and the force-dependent unfolding and refolding of Ig domains[11–14].

Our current understanding of the force-dependent unfolding and refolding dynamics of I-band Ig domains is largely based on extensive studies of the titin I27 (also known as I91) domain located at the distal region of the I-band[11,12,14–22]. While the I-band Ig domains of titin exhibit highly conserved structural features–characterized by a two-layer sandwich of seven β-strands, where the 1st (A) and 7th (G) strands are in close proximity, resulting in a shearing-force stretching geometry[23]–there is also evidence suggesting heterogeneity in the mechanical responses of these domains[13]. Therefore, it is essential to systematically quantify the mechanical responses of Ig domains, particularly in the proximal and middle regions, to gain a comprehensive understanding of the mechanical properties of the titin I-band.

[1]Department of Physics, Research Institute for Biomimetics and Soft Matter, Fujian Provincial Key Lab for Soft Functional Materials Research, Xiamen University, Xiamen, China. [2]Department of Biochemistry and Division of Orthopaedic Surgery of the Second Affiliated Hospital, Zhejiang University School of Medicine, Hangzhou, China. [3]State Key Laboratory for Cellular Stress Biology, School of Life Sciences, Xiamen University, Xiamen, China. [4]Center of Biomedical Physics, Wenzhou Institute, University of Chinese Academy of Sciences, Wenzhou, China. ✉e-mail: chenhu@xmu.edu.cn; yu.miao@zju.edu.cn; leshimin@xmu.edu.cn

Interestingly, the majority (~80%) of the I-band Ig domains feature two or more evolutionarily conserved cryptic cysteines (Supplementary Figs. 1–3), which have the potential to be regulated by oxidative stress. In contrast, Ig domains in the A-band and M-line typically contain only one cysteine[24]. Notably, cysteines within the I-band Ig domains have been suggested to form disulfide bonds under oxidative stress. This phenomenon can lead to alterations in the mechanical responses of titin Ig domains[25]. A comprehensive and quantitative understanding of how disulfide bonds impact the mechanical behavior of Ig domains is crucial for unraveling the mechanical properties of titin under oxidative stress.

Moreover, proline isomerization has emerged as a highly effective regulatory mechanism in a wide array of biological processes[26–32]. Due to its cis-trans conformational switches, proline residues significantly influence the folding kinetics and conformational dynamics of proteins[33–35]. While trans-state prolines dominate in most native protein conformations, instances of cis-state prolines or a combination of both cis and trans states have been documented[28–30,32,33,36,37]. This results in two distinct native states[29,30,32,37]. Regulation via proline isomerization is particularly crucial for mechanosensitive proteins that experience physiological mechanical forces, as these forces can trigger or facilitate conformational changes in the protein, potentially promoting proline isomerization. In turn, proline isomerization modulates the force responses of the protein[32].

Intriguingly, in the proximal and middle titin I-band region, over 60% of the Ig domains contain a proline in the cis-state based on solved crystal structures and AlphaFold-structural predictions (see Methods section: AlphaFold based structural prediction, Supplementary Figs 1–11)[38–45]. For example, the Ig1 (Ig-like 10, 2078–2167 residues of human titin) domain at the very proximal region of the force-bearing titin I-band contains a proline (P2105) in the cis-state in the solved crystal structure[38]. The P2105 is located at the loop bridging the 2nd (B) and the 3rd (C) strands. An interesting question is whether physiologically relevant mechanical forces on the Ig1 domain could trigger or facilitate potential cis-trans transitions due to the force-induced conformational dynamics of Ig1. Moreover, near the P2105, a cysteine residue (C2109) is located within the 3rd (C) strand and may potentially form a disulfide bond with the other cysteine residue (C2134) on the 5th (E) strand, thereby locking 24 amino acids within the disulfide bond. This raises intriguing questions about how disulfide bond formation might affect the mechanical responses of Ig1 and its potential impact on proline isomerization within the Ig1 domain.

In this work, to address the aforementioned questions and gain a quantitative understanding of the potential interplay among proline isomerization, disulfide bonds, and mechanical forces affecting the conformational dynamics of the mechanosensitive titin I-band proximal Ig1 domain, we conducted a direct and systematic quantification of the force-dependent conformational dynamics of Ig1 using a home-built magnetic tweezers setup[46,47]. Our findings reveal several key insights. In both the reduced and oxidized states of Ig1, proline isomerization leads to two distinct native states with differing mechanical and thermal stability. The trans-Ig1 is approximately 1000 times less resistant to force-dependent unfolding, exhibits unfolding forces that are about 50 pN lower, and has a zero-force folding free energy that is 10 − 13 k_BT lower than the cis-Ig1. Reduced cis- and trans-Ig1 display a nonmonotonic catch-slip bond unfolding behavior, which can be explained by a one-pathway model with a force-dependent flexible transition distance. Oxidized cis- and trans-Ig1 exhibit an unexpected nonmonotonic slip-catch-slip bond unfolding behavior, which can be attributed to the presence of an additional hidden intermediate state promoted by the disulfide bond. Importantly, we also demonstrated that the proline isomerization-induced formation of two distinct native states is likely a shared feature among the majority of the I-band Ig domains. Altogether, this study provides detailed insights into the molecular mechanisms underlying the force-dependent conformational dynamics of titin Ig1, showcasing a remarkably effective modulation of two binary switches (proline isomerization and disulfide bond) in regulating critical mechanosensitive proteins within the physiological force range.

Results

Proline isomerization induces two distinct native states for both reduced and oxidized titin Ig1

To investigate the force-dependent dynamics of the titin Ig1 domain, we designed a protein construct that includes (from N-terminus to C-terminus) a biotinylated AviTag, titin Ig1, and a SpyTag (see Methods section: Plasmids preparation and protein expression). This design allows for specific tethering of the titin Ig1 domain between a streptavidin-coated super-paramagnetic bead and a SpyCatcher-coated coverslip surface in a flow channel (Fig. 1a)[48,49]. A magnetic tweezers setup was employed to apply well-controlled force to the tethered Ig1 and to record real-time molecular extension changes, which are inferred from changes in bead height (Fig. 1a, right panel)[46,47,50] (see Methods section: Single-protein manipulation).

Figure 1 a, bottom right panel, illustrates a typical linear force-loading experiment procedure, where the force applied to the tethered molecule is linearly increased from 1 pN to 70 pN at a rate of 1 pN s^{-1}. This is followed by a rapid reduction in force to 10 pN and a subsequent linear decrease at a rate of − 1 pN s^{-1}. During the force-increase scan, the folded domain undergoes force-induced unfolding, as indicated by the stepwise increase in bead height (upward arrows). Conversely, the unfolded domain refolds at low forces ≤ 5 pN during the force-decrease scan (e.g., Fig. 1a, bottom right panel), allowing for repeated force scans through multiple cycles on a single tethered molecule. A characteristic ~4 nm stepwise extension fluctuation at ~30 pN, resulting from the unzipping/rezipping dynamics of the SpyTag from the SpyCatcher, was consistently observed (inset in the panel, also detailed in Supplementary Fig. 12). This signal serves as a positive control for single-molecule tethering and provides an additional force-calibration reference 51.

Figure 1b, left panel, displays the typical force–bead height curves of titin Ig1 in its reduced state during linear force-increase scans, ranging from ~1 pN to ~70 pN, with a loading rate of 1 pN s^{-1}. In each scan, the Ig1 domain unfolding event is observed as a stepwise increase in bead height (arrows in Fig. 1b). Figure 1b, middle and right panels, show the resulting force-dependent unfolding step sizes and the normalized unfolding force distributions, respectively. The observed force-dependent unfolding step size is consistent with theoretical step size calculations where the unfolded Ig1 is considered as a peptide chain with 95 amino acids based on the worm-like chain model[52], while the folded Ig1 is considered as a rigid body (Fig. 1b, see Methods section: Theoretical calculation of transition step sizes).

Interestingly, two distinct mechanical groups of Ig1 were observed (Fig. 1b). One group, mechanically stronger, unfolds at forces of 61.7 ± 5.3 pN (mean ± std), while the mechanically weaker group unfolds at forces of 5.3 ± 0.9 pN. We hypothesize that these two distinct mechanical groups result from the P2105 cis-trans isomerization. To test this, we performed similar linear force-loading experiments on two Ig1 proline point-mutant constructs, Ig1^{P2105A} and Ig1^{P2105G}, where at 2105 position, proline was mutated to alanine, and glycine, respectively (see Methods section: Plasmids preparation and protein expression). The resulting force–bead height curves, force–step size curves, and the normalized unfolding forces distributions of the two mutant constructs are plotted in Fig. 1c–d, respectively. Consistent with our hypothesis, the unfolding of Ig1^{P2105A} and Ig1^{P2105G} primarily shows a single mechanical group (4.9 ± 1.9 pN, and 6.9 ± 2.0 pN) similar to the weaker one observed in wild-type Ig1. Together, these results demonstrate that the P2105 cis-trans isomerization gives rise to two distinct native states of Ig1, each

https://doi.org/10.1038/s41467-025-57989-y

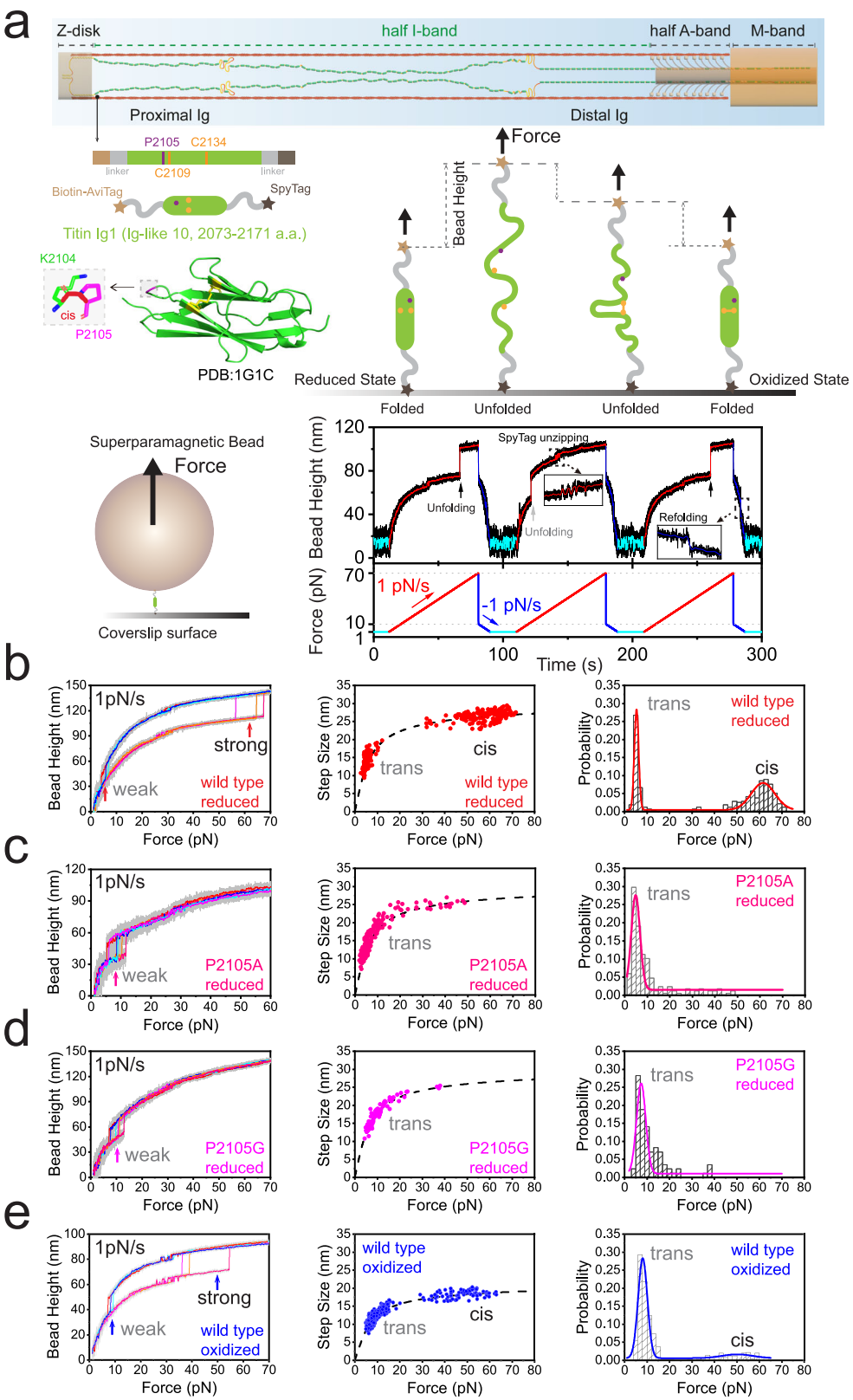

associated with different mechanical stability. The cis state of proline in Ig1 confers high mechanical stability to the domain, while the trans-state switches the domain into a much weaker mechanical state. Here, we note that the slight differences in the peak unfolding forces between the mutated constructs and wild-type trans-Ig1 are possibly due to the subtle changes in mechanical stability caused by the point mutations.

Next, to determine whether the two native states of Ig1, which depend on proline isomerization, are also present when the nearby cysteine disulfide bond is formed (i.e., in oxidized Ig1), we performed similar linear force-loading scans on wild-type Ig1 in the absence of a reducing agent, such as dithiothreitol (DTT), in buffered solution. After several scan cycles, the cysteine disulfide bond formed, as indicated by a shortening of the force-dependent unfolding step size, consistent

https://doi.org/10.1038/s41467-025-57989-y

Fig. 1 | Proline cis-trans isomerization induces two distinct native states of Ig1 in both reduced and oxidized states. a Illustration of the single-molecule experiments design for probing titin Ig1 mechanics. Left panel: the single-molecule construct design of titin Ig1 and Ig1 structure illustration (PDB:1G1C) where the P2105 in the cis state is highlighted. Right panel: the illustration of the force-dependent height changes of titin Ig1. Bottom panel: Representative time-bead height curves during linear force-loading cycles. **b**–**e** Left panels: Representative force--bead height curves of the titin Ig1 during linear force-increase scans with a loading rate of 1 pN s^{-1}, for reduced Ig1 (**b**), P2105A mutation of Ig1 in the reduced state (**c**), P2105G mutation of Ig1 in the reduced state (**d**), and the oxidized state (disulfide bond formed) Ig1 (**e**), respectively. The raw data (gray) is 10-point FFT smoothed (colored lines). The cis- and trans-states are superimposed on the same plot for direct comparison. Middle panels: The resulting force--step size distributions of the Ig1 unfolding events obtained from the linear scans, the dashed curves are the theoretical calculation of force-dependent step sizes for reduced or oxidized Ig1. Right panels: The resulting normalized unfolding force distributions (bin-size = 2) of the Ig1 in corresponding conditions. The number of data points for the statistics are $N = 314$, 168,85, and 409, respectively. The colored lines are the double-Gaussian or Gaussian fitting of the distributions, giving the peak forces as 5.3 ± 0.9 pN and 61.7 ± 5.3 pN (**b**), 4.9 ± 1.9 pN (**c**), 6.9 ± 2.0 pN (**d**), and 8.1 ± 2.1 pN and 50.2 ± 6.8 pN (**e**).

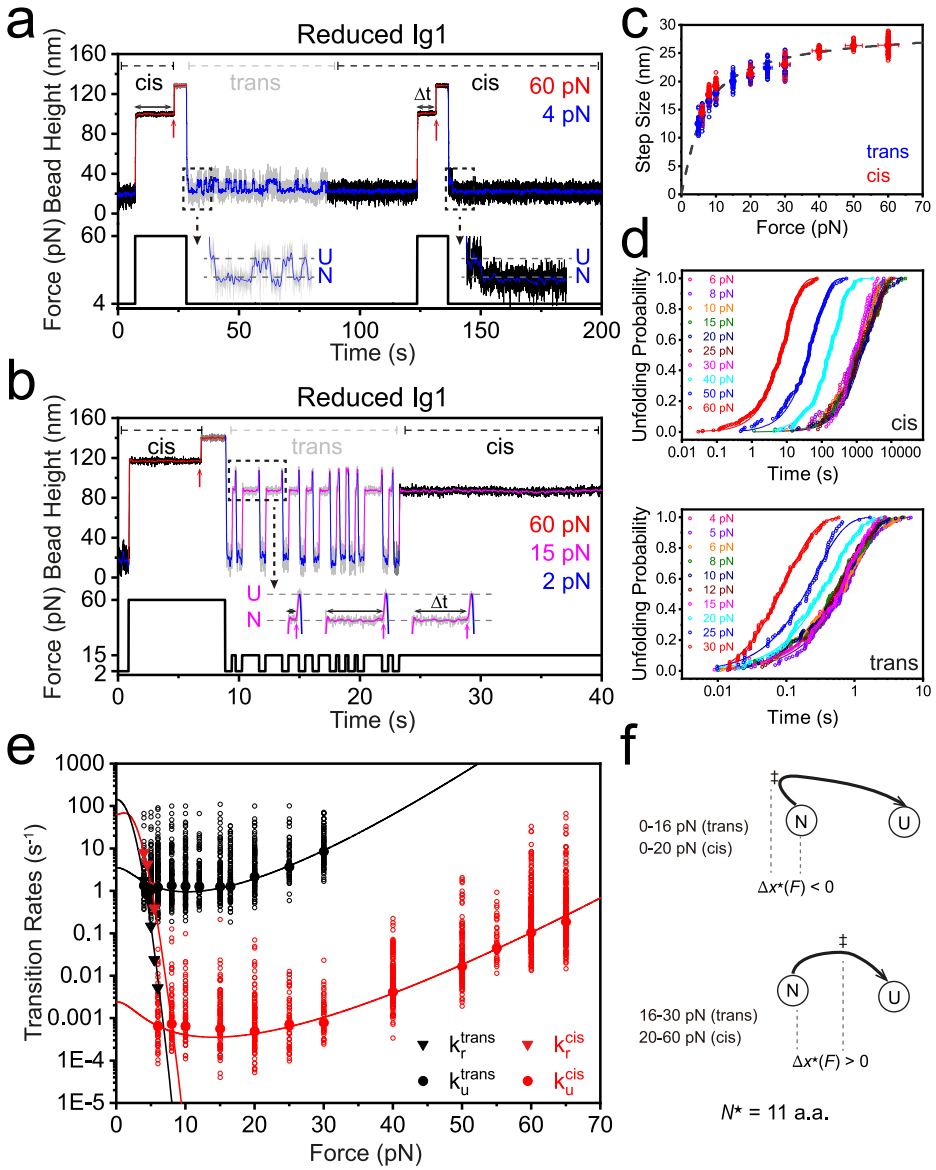

Fig. 2 | The force-dependent unfolding and refolding rates of cis and trans Ig1 in reduced state. a, **b** Typical time-bead height curves of reduced Ig1 during force-jump experiments between different forces (colored lines). The cis or trans-state of the proline is roughly indicated by the black or gray color of the raw data. The unfolding event of the Ig1 at 60 pN at each cycle was indicated by a red arrow. **c** The force-dependent unfolding step sizes of the reduced Ig1 domain at trans or cis state during the force-jump measurement. The dashed line is a theoretical calculation of the force-dependent step size of reduced Ig1. Solid circles show the mean step size at each force; hollow circles show experimental values ($n > 20$). Vertical error bars indicate the standard deviation (std); horizontal error bars represent a 5% force uncertainty. **d** The time-evolution of the unfolding probability of the Ig1 in cis or trans states at different forces. **e** Force-dependent unfolding (circles) and refolding (triangles) rates of the reduced Ig1 in cis and trans states. The hollow circles are individual unfolding rates measured ($n > 40$), and the solid circles are the characterized unfolding rates at the force obtained by fitting in panel (**d**). The lines are fitting curves with the one-pathway model with force-dependent transition distance. **f** A sketch of the one-pathway theoretical model, where the transition distance between N and U states is force-dependent, due to the force-dependent extension of the transition state flexible peptide. The estimated number of amino acids peeled off during the transition state (N*) is indicated in the panel. The highest energy barrier position is indicated by ‡.

https://doi.org/10.1038/s41467-025-57989-y

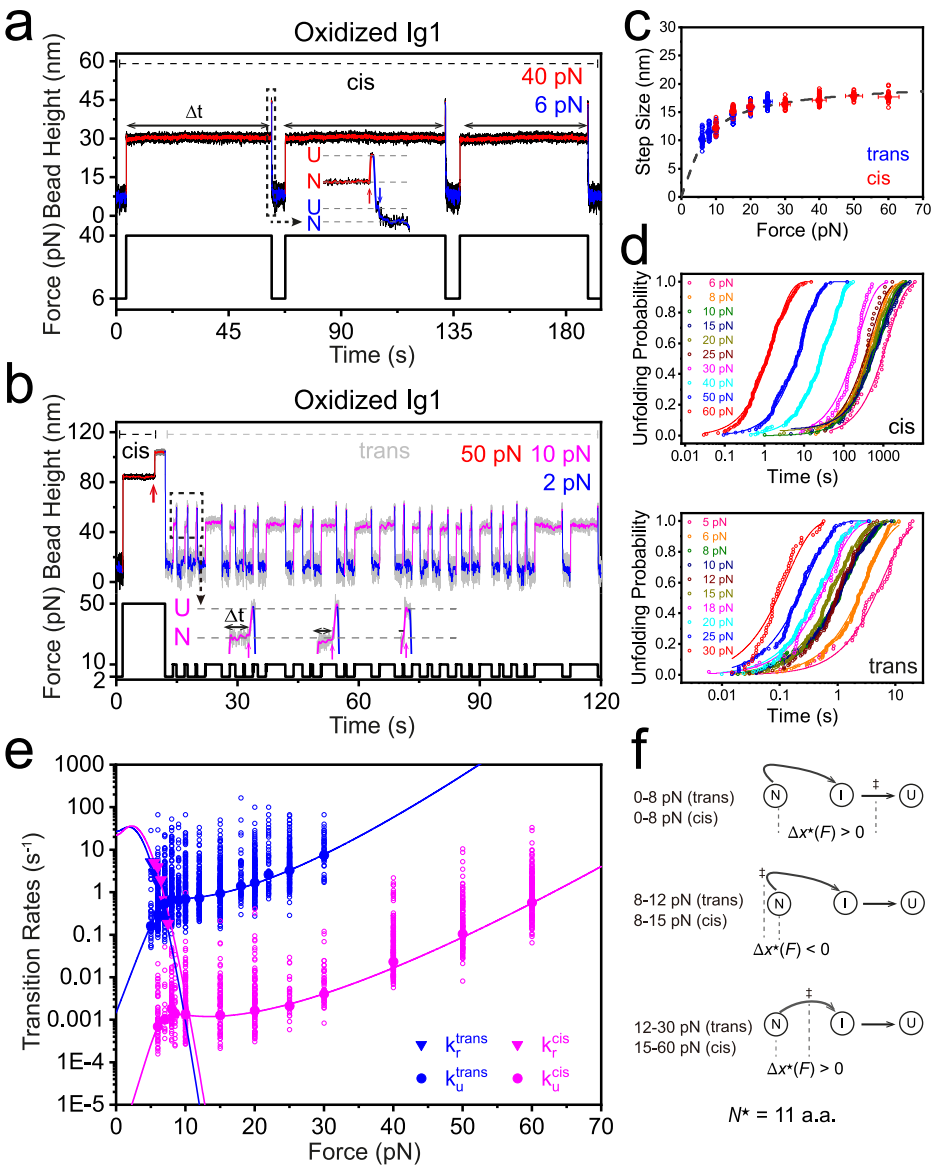

Fig. 3 | The force-dependent unfolding and refolding rates of cis and trans Ig1 in oxidized state where disulfide bond formed. a, **b** Typical time-bead height curves of oxidized Ig1 during force-jump experiments between different forces (colored lines). The cis or trans-state of the proline is roughly indicated by the black or gray color of the raw data. Example unfolding events of the Ig1 at 40 pN (red arrow), 50 pN (red arrow), or 10 pN (magenta arrows), and the example refolding events of Ig1 at 6 pN (blue arow) are indicated. **c** The force-dependent unfolding step sizes of the oxidized Ig1 domain at trans or cis state during the force-jump measurement. The dashed line represents the theoretical calculation, while solid and hollow circles denote the mean step size and experimental values ($n > 20$), respectively. Vertical error bars indicate the standard deviation (std), while horizontal error bars represent a 5% force uncertainty. **d** The time-evolution of the unfolding probability of the Ig1 in cis or trans states at different forces. **e** Force-dependent unfolding (circles) and refolding (triangles) rates of the oxidized Ig1 in cis and trans states. The hollow circles are individual unfolding rates measured ($n > 20$), and the solid circles are the characterized unfolding rates at the force obtained by fitting in panel (**d**). The lines are fitting curves with the one-pathway model with force-dependent transition distance and a hidden intermediate state. **f** A sketch of a one-pathway theoretical model with a hidden intermediate state. In the model, there is a hidden intermediate state (I) between the N and U states. The transition distance between N and I states is force-dependent, due to the force-dependent extension of the transition state flexible peptide. The estimated number of amino acids peeled off during the N-I transition (N*) is indicated in the panel. The highest energy barrier position is indicated by ‡.

with theoretical step size calculations showing 24 amino acids locked in the disulfide bond (Supplementary Fig. 13; see Methods section: Theoretical calculation of transition step sizes). Figure 1d shows the typical force–bead height curves of titin Ig1 in its oxidized state with a disulfide bond (left panel), the resulting force-dependent step sizes (middle panel), and the normalized unfolding force distribution (right panel). Notably, even in the oxidized state, Ig1 exhibits proline isomerization, leading to two distinct native states with unfolding forces peaking at 8.1 ± 2.1 pN and 50.2 ± 6.8 pN, respectively. Interestingly, the disulfide bond appears to reduce the mechanical stability of the cis-Ig1 state while enhancing the mechanical stability of the trans-Ig1 state (Supplementary Table 1).

Catch-slip bond force-dependent unfolding behavior of both reduced cis- and trans-Ig1

To further quantitatively understand the effects of both disulfide bonds and proline isomerization on the mechanical stability of Ig1, we aimed to directly quantify the force-dependent unfolding and refolding rates of Ig1 in its cis or trans and reduced or oxidized states by implementing force-jump scan cycles. To probe the force-dependent

unfolding rate of reduced cis-Ig1, each force-jump scan cycle began by holding the folded Ig1 at ≤ 4 pN to maintain it in the cis state. The force was then rapidly increased to a target level and maintained until unfolding was observed (e.g., 60 pN, Fig. 2a, red arrow), from which the domain's dwell time (Δt) at that force was recorded. The force was subsequently reduced to ~4 pN to allow Ig1 to refold. If the Ig1 was in the trans-state, it would dynamically unfold and refold for tens of seconds until transitioning to the more mechanically stable cis state (e.g., cycle 1 in Fig. 2a). If the Ig1 was in the cis state, it refolded rapidly at this force (e.g., cycle 2 in Fig. 2a). Once the Ig1 transitioned to the cis state, the force was again increased to the target level, initiating the next force-jump scan cycle. By repeating multiple force-jump scan cycles across a wide range of forces, we obtained the force-dependent dwell times of the domain. Analyzing the time evolution of the domain's unfolding probabilities at each force (Fig. 2d) allowed us to determine the force-dependent unfolding rates of reduced cis-Ig1 (Fig. 2e).

Next, we implemented a modified force-jump scan cycle to quantify the force-dependent unfolding rates of trans-Ig1 (Fig. 2b). The force was initially increased to 60 pN to mechanically unfold cis-Ig1, maintaining this force for several seconds to allow for the proline cis-trans transition in the unfolded state. The force was then dropped to a low level (e.g., 2 pN) for approximately one second to facilitate rapid refolding of trans-Ig1. After refolding, the force was increased to a target level and maintained until Ig1 unfolded (e.g., 15 pN in the panel, Fig. 2b). The force-jump cycles were repeated between 2 pN (low force) and 15 pN (target force) until the proline transitioned back to the cis state, indicated by a significantly prolonged lifetime at the target force (Fig. 2b). The force was then increased to ~60 pN to restart the trans-Ig1. By repeating the scan cycles at a wide range of target forces, we obtained the force-dependent unfolding rates of reduced trans-Ig1 (Fig. 2d, e and Supplementary Fig. 14).

Figure 2 e shows the resulting force-dependent unfolding rates of both reduced cis-Ig1 and trans-Ig1. Clearly, the mechanical stability of trans-Ig1 decreases by approximately 1000-fold compared to cis-Ig1 across physiological force ranges. Intriguingly, both trans- and cis-Ig1 exhibit non-monotonic force-dependent catch-bond to slip-bond unfolding behavior in their reduced states. At forces ≤16 pN (trans) or ≤ 20 pN (cis), the Ig1 unfolding rate decreases as force increases (catch-bond). At higher forces, the unfolding rate increases with force (slip-bond).

The catch-slip behavior of Ig1 unfolding can be explained by a one-pathway model with a force-dependent flexible transition distance (Fig. 2f)[12,14,53,54]. Based on previous steered molecular dynamics (SMD) simulations of titin Ig domains[55–57], it can be assumed that domain unfolding primarily follows a transition pathway involving the peeling of the A-A' strand, during which bonded residues in the A-A' strand are sequentially peeled off from the remaining folded core until the transition state is reached. The transition state likely contains a flexible peptide with $N^\star$ residues and a remaining folded core. The transition distance of the domain is $\Delta x^*(F) = x^*_{\text{peptide}}(F) + x^*_{\text{core}}(F) - x^0(F)$, where $x^*_{\text{peptide}}(F)$ can be described by the worm-like chain model[52], with a contour length of $L^\star = N^\star \times l_0$ and a bending persistence length $A = 0.4 - 0.8$ nm; $l_0 = 0.38$ nm is the contour length per residue[11,17]. $x^*_{\text{core}}(F)$ and $x^0(F)$ can be described by a force-dependent single rigid body rotation model with rigid body lengths $b^\star$ and b_0, respectively, which can be measured from the structure[38]. The force-dependent unfolding rate of the domain can then be fitted using the Arrhenius Law (black and red lines, Fig. 2e): $k_u(F) = k_u^0 \exp\left(-\frac{\Delta G^*(F)}{k_B T}\right)$, where $\Delta G^*(F) = -\int_0^F \Delta x^*(f) df$ is the force-dependent free energy difference between the transition and native states. We obtained $N^\star = 11$ for both trans-Ig1 and cis-Ig1 (Supplementary Table 2), suggesting that the transition state likely involves the complete peeling off of the A strand while the A' strand remains bonded, which is consistent with previous SMD simulations on titin Ig1[57]. Here we note that the catch-slip behavior of Ig1 unfolding can also be explained by a two-pathway model in general that includes a force-resistant pathway at lower forces and a force-compliant pathway at higher forces (Supplementary Note 2, and Supplementary Fig. 15)[58].

Slip-catch-slip bond force-dependent unfolding behavior of both oxidized cis- and trans-Ig1

Next, we investigated the force-dependent unfolding rates of cis-Ig1 and trans-Ig1 in their oxidized state (i.e., when the disulfide bond is formed). Programmed force-jump scan cycles were applied to the oxidized cis-Ig1 (Fig. 3a) and trans-Ig1 (Fig. 3b). The resulting force-dependent unfolding rates for both cis-Ig1 and trans-Ig1 in the oxidized state were determined by analyzing the dwell time of the domains at each force (Fig. 3c–d), and are plotted in Fig. 3e. Notably, in the oxidized state, the mechanical stability of trans-Ig1 also shows a dramatic decrease (by approximately 1000-fold) compared to cis-Ig1 over the physiological force range.

Unexpectedly, both cis-Ig1 and trans-Ig1 in the oxidized state exhibit non-monotonic slip-catch-slip unfolding behavior. At forces ≤ 8 pN, the Ig1 unfolding rate increases as force increases (slip-bond). Between 8 − 15 pN for cis-Ig1 and 8 − 12 pN for trans-Ig1, the unfolding rate decreases as force increases (catch-bond). At higher forces, the unfolding rate again increases with force (slip-bond). For the oxidized Ig1, we fitted the force-dependent unfolding rates in the first slip-bond regime (0 − 8 pN) and the second slip-bond regime (15 − 30 pN for trans-Ig1, and 25 − 60 pN for cis-Ig1) using Bell's model, yielding Δx_u and k_u^0 for each regime. The oxidized Ig1 shows an additional larger positive $\Delta x_u = 2.45$ nm (trans) or 2.07 nm (cis) in the first slip-bond regime (0 − 8 pN). This suggests the existence of an intermediate state (I) between the native state (N) and the unfolded state (U).

By incorporating an additional hidden transient intermediate state into the one-pathway model, featuring a force-dependent flexible transition distance, the slip-catch-slip behavior of the oxidized Ig1 domain can be accurately described using the modified model (Fig. 3f)[53,58,59] (Supplementary Table 3). In this model (Fig. 3f), the transition distance for the N-I transition, $\Delta x^*_{NI}(F)$, is force-dependent due to the force-dependent nature of the transition state length (as detailed for the reduced Ig1). On the other hand, the transition distance for the I-U transition, Δx^*_{IU}, is a positive value. The energy barrier heights for both the N-I and I-U transitions are influenced by changes in force.

At forces ≤ 8 pN for both trans and cis states, the highest energy barrier along the N-U transition (i.e., the transition state, denoted by ‡ in the panel) lies along the I-U transition path (Fig. 3f, top panel). In this range, the transition distance, $\Delta x^*(F) > 0$, leading to slip-bond unfolding behavior (top panel). At forces ≥ 8 pN, the highest energy barrier along the N-U transition shifts now locates along the N-I transition path. In this regime, the transition distance becomes $\Delta x^*(F) = \Delta x^*_{NI}(F)$, which is negative at forces < 12 pN (trans) or < 15 pN (cis), resulting in catch-bond unfolding behavior (middle panel) in the force range of 8–12 pN (trans) or 8–15 pN (cis). In the force regime of > 12 pN (trans) or > 15 pN (cis), the transition distance becomes positive again, giving rise to the second slip-bond unfolding behavior (bottom panel).

In addition, we investigated the refolding dynamics of Ig1 by performing force-jump-scan cycles or equilibrium force measurements. The resulting force-dependent refolding rates for Ig1 in the reduced or oxidized, cis or trans states are shown in Figs. 2e and 3e, with zero-force folding kinetic parameters obtained by fitting the experimental data to the Arrhenius law: $k_r(F) = k_r^0 \exp\left(-\frac{\Delta G^*(F)}{k_B T}\right)$ (see Methods section: Arrhenius Law analysis of force-dependent refolding rates). In both the reduced and oxidized states, the refolding rate of

https://doi.org/10.1038/s41467-025-57989-y

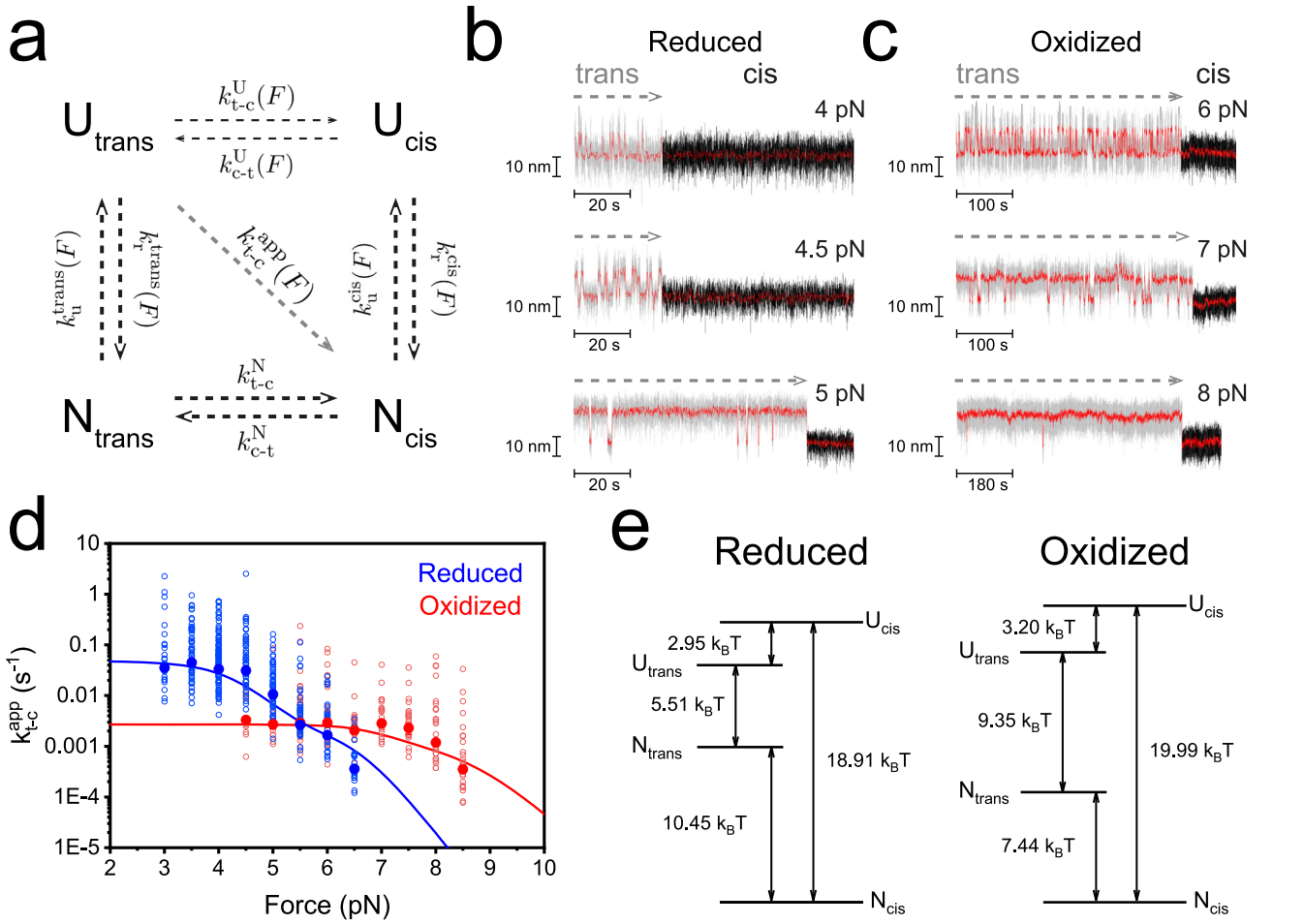

Fig. 4 | The effects of force and oxidization on proline isomerization. a Diagram of proline cis-trans isomerization transition kinetics of Ig1. There are two possible kinetic paths from the U_{trans} state to the N_{cis} state: (i) from U_{trans} to U_{cis}, and then to N_{cis} state, or (ii) from U_{trans} to N_{trans}, and then to N_{cis} state. The two paths result in an apparent transition rate of $k_{t\text{-}c}^{app}(F)$. **b**, **c** Representative time traces of unfolded trans to folded cis transition at different forces for reduced Ig1 (**b**) and oxidized Ig1 (**c**). The dashed arrows indicate the example dwell times measured to calculate the $k_{t\text{-}c}^{app}(F)$. **d** The resulting force-dependent apparent trans-cis transition rate for reduced Ig1 (blue) and oxidized Ig1 (red). Hollow circles represent experimental values ($n > 15$), while solid circles denote the apparent trans-cis rates obtained from single-exponential fitting of the experimental data. Horizontal error bars indicate the standard deviation. The lines are theoretically fitting using Equation 1 with sets of possible parameters. **e** The zero-force free energy difference (ΔG) of the Ig1 in different states. The $\Delta G_0^{cis} = 18.91 \pm 0.30\ k_BT$ (reduced)or $= 19.99 \pm 0.37\ k_BT$ (oxidized), and $\Delta G_0^{trans} = 5.51 \pm 0.10\ k_BT$ (reduced)or $= 9.35 \pm 0.12\ k_BT$ (oxidized), are obtained based on the experimentally measured force-dependent unfolding/refolding rates at each state. The $\Delta G_{t\text{-}c}^{N} = 10.45 \pm 0.58\ k_BT$ (reduced)or $= 7.44 \pm 0.71\ k_BT$ (oxidized), and $\Delta G_{t\text{-}c}^{U} = 2.95 \pm 0.19\ k_BT$ (reduced)or $= 3.20 \pm 0.23\ k_BT$ (oxidized) are obtained based on the theoretical fitting of the apparent trans-cis transition rate using Equation 1. The mean and standard deviation of each value are obtained by bootstrap analysis[65].

the cis-state Ig1 is faster than that of the trans-state Ig1 at a given applied force (Figs. 2e and 3e). Additionally, for both trans and cis states, the refolding rate of the oxidized Ig1 is faster than that of the reduced Ig1 under the same applied force (Figs. 2e and 3e and Supplementary Fig. 14). These findings suggest that both trans-cis isomerization and disulfide bond formation promote refolding of the domain.

Effects of disulfide bond and forces on proline isomerization

Next, we aimed to quantify the force-dependent proline isomerization rates in both the reduced and oxidized states. We measured the apparent transition rate, $k_{t\text{-}c}^{app}(F)$, which represents the transition rate from the trans unfolded state (U_{trans}) to the cis folded state (N_{cis}) (Fig. 4a–d). This apparent transition rate, $k_{t\text{-}c}^{app}(F)$, is related to the transition rates between the trans-cis and cis-trans states in the native and unfolded states, $k_{t\text{-}c}^{U}(F)$, $k_{t\text{-}c}^{N}$ and $k_{c\text{-}t}^{U}(F)$ as given by the following expression[60] (see Methods section: Apparent proline isomerization rate analysis):

$$k_{t\text{-}c}^{app}(F) = \left(1 - P_{U,t}(F)\right)k_{t\text{-}c}^{N} + P_{U,t}(F)\frac{k_{t\text{-}c}^{U}(F)k_{r}^{cis}(F)}{k_{t\text{-}c}^{U}(F) + k_{r}^{cis}(F) + k_{c\text{-}t}^{U}(F)} \quad (1)$$

Here, the $P_{U,t}(F)$ is the measured force-dependent probability of the trans unfolded state $k_r^{cis}(F)$ is the measured force-dependent refolding rate of the domain in the cis state. The constant $k_{t\text{-}c}^{N}$ is force-independent, as the proline in the folded state is not subjected to additional mechanical force. In contrast, $k_{t\text{-}c}^{U}(F)$ and $k_{c\text{-}t}^{U}(F)$ are force-dependent since the proline in the unfolded domain is directly affected by mechanical stretching. These rates can be described by Bell's model[61]: $k_i^U(F) = k_i^{U,0}\exp(\frac{F\Delta x_i}{k_BT})$, where i denotes either the trans-cis (t-c) or cis-trans (c-t) transition, the $k_i^{U,0}$ and Δx_i represent the zero-force transition rate and the transition distance for the corresponding

transition, respectively. To obtain $|\Delta x_i|$, we measured the force-dependent cis-trans isomerization rate, $k^{U}_{c\text{-}t}(F)$, at several forces for both reduced and oxidized Ig1 (Supplementary Figs 16 and 17). Fitting the data to Bell's model above yields $k^{U,0}_{c\text{-}t} = (4.3 \pm 1.5) \times 10^{-2}$ s^{-1} and $\Delta x_{c\text{-}t} = 0.20 \pm 0.02$ nm (Supplementary Fig. 17). By assuming symmetric transition distances between the unfolded cis and trans states, we obtained $|\Delta x_i| = 0.20 \pm 0.02$ nm.

Fitting Eq. (1) to the experimental data for both reduced and oxidized Ig1, we obtained $k^{U,0}_{t\text{-}c} = (2.26 \pm 0.22) \times 10^{-3}$ s^{-1} and $k^{N}_{t\text{-}c} = (4.94 \pm 0.41) \times 10^{-2}$ s^{-1} for reduced Ig1, and $k^{U,0}_{t\text{-}c} = (1.28 \pm 0.20) \times 10^{-3}$ s^{-1} and $k^{N}_{t\text{-}c} = (2.70 \pm 0.29) \times 10^{-3}$ s^{-1} for oxidized Ig1 (Fig. 4d and Supplementary Fig. 17). In addition, kinetic simulations using the above transition rate parameters also provide $k^{app,sim}_{t\text{-}c}(F)$, which is in good agreement with the experimental results (Supplementary Note 3 and Supplementary Fig. 18). Interestingly, $k^{N}_{t\text{-}c}$ for oxidized Ig1 is over 10 times smaller than that for reduced Ig1, whereas $k^{U}_{t\text{-}c}$ for oxidized Ig1 is comparable to that of reduced Ig1. This suggests that the oxidation (disulfide bond formation) of nearby cysteine residues significantly slows down the trans-cis isomerization of proline in the folded states.

Effects of proline isomerization and disulfide bond on thermostability of Ig1

The zero-force folding free energy of Ig1 can be obtained using the following expression:

$$\Delta G_0 = \Delta G(F) + \int_0^F \Delta x_{UN}(f)df \tag{2}$$

where $\Delta G(F) = k_B T \ln \frac{k_f(F)}{k_u(F)}$ represents the force-dependent protein folding free energy, and $\Delta x_{UN}(f)$ is the force-dependent extension difference of Ig1 between the unfolded and folded states. The zero-force isomerization free energy for both the unfolded and folded states can be derived as:

$$\Delta G^{U}_{t\text{-}c} = k_B T \ln \frac{k^{U}_{t\text{-}c}}{k^{U}_{c\text{-}t}} \tag{3}$$

$$\Delta G^{N}_{t\text{-}c} = \Delta G^{cis}_0 - \Delta G^{U}_{c\text{-}t} - \Delta G^{trans}_0 \tag{4}$$

The resulting free energy differences for each state are summarized in Fig. 4e. Interestingly, in the cis-proline state, the zero-force folding free energy ΔG_0 of oxidized Ig1 (19.99 k_BT) is slightly (~1 k_BT) higher than that of the reduced Ig1 (18.91 k_BT). In contrast, in the trans-proline state, ΔG_0 of oxidized Ig1 (9.35 k_BT) is significantly (3.84 k_BT) higher than that of reduced Ig1 (5.51 k_BT). These results suggest that the disulfide bond enhances the thermostability of trans-Ig1 while having a much smaller effect on the thermostability of cis-Ig1. In sharp contrast, ΔG_0 of cis-Ig1 is 13.4 k_BT higher than that of trans-Ig1 for reduced Ig1, and 10.64 k_BT higher for oxidized Ig1, indicating that trans-cis isomerization significantly enhances the thermostability of both reduced and oxidized Ig1.

The free energy differences of proline isomerization are also estimated based on Boltzmann distribution (Fig. 4e). Similar values of $\Delta G^{U}_{c\text{-}t} \sim 3\, k_BT$ were estimated for both reduced and oxidized Ig1. This value is slightly larger than the previously estimated value of approximately 2 k_BT between cis-FLNa20 and trans-FLNa20[32]. We speculate that the slight difference may either arise from experimental variability within a reasonable range or result from the influence of neighboring residues[62]. In contrast, it appears that disulfide bond formation lowers the free energy differences of proline isomerization in the folded state. In addition, based on these free energy difference estimations, the force-dependent probability of Ig1 in each state (cis or trans, unfolded or folded) can be calculated using the Boltzmann distribution (Supplementary Fig. 18 and Supplementary Table 5).

Proline isomerization induced two distinct native states are likely conserved among titin Ig domains

More than 60% of the Ig domains within the proximal and middle regions of the titin I-band contain a proline in the cis-state, based on resolved crystal structures and/or AlphaFold structural predictions (Supplementary Figs 1–4)[38–43,45]. In stark contrast, the distal region of the titin I-band contains only 7% cis-proline Ig domains (Fig. 5a). This observation suggests that the cis-proline-containing Ig domains in the proximal and middle I-band regions may exhibit two mechanically distinct native states due to proline isomerization. In other words, the proline isomerization-mediated transition between these two states is likely highly conserved among the Ig domains of the proximal and middle I-band regions of titin. To test this hypothesis, we randomly selected another cis-proline-containing Ig domain (Ig-like 32) from the middle region of the I-band and investigated its mechanical behavior through linear force-loading experiments. Consistent with our hypothesis, Ig-like 32 also displays two distinct mechanical peaks during force-loading: one at 9.3 ± 4.1 pN and another at 64.3 ± 2.3 pN (Fig. 5b–e). Figure 5f illustrates the representative dynamics of cis-unfolding of Ig-like 32 at 60 pN, a cis-refolding event at 3 pN, and the transition between a dynamically unfolded/refolding trans-Ig-like 32 and a folded cis-Ig-like 32 at 3 pN.

Discussion

In summary, we have systematically investigated how proline isomerization and disulfide bonds collectively regulate the kinetics and dynamics of titin Ig1 under physiological forces. Our findings reveal that proline isomerization gives rise to two mechanically distinct native states of Ig1: the mechanically weak trans-Ig1 and the mechanically strong cis-Ig1, both in the reduced and oxidized states. In the reduced state, both cis- and trans-Ig1 exhibit a catch-slip bond unfolding behavior, which can be explained by a one-pathway model featuring a force-dependent, flexible transition distance. In the oxidized state, both cis- and trans-Ig1 display a slip-catch-slip bond unfolding behavior, which can be attributed to an additional hidden intermediate state stabilized by the disulfide bond. Taken together, this study provides detailed insights into the molecular mechanisms underlying the force-dependent conformational dynamics of titin Ig1, demonstrating the remarkably effective modulation of two binary switches–proline isomerization and disulfide bonding–in the regulation of critical mechanosensitive proteins under physiological force conditions.

In the proximal and middle regions of the titin I-band, more than 60% of the Ig domains are in the cis-state for proline, as indicated by crystal structures[38–43] and AlphaFold3 structural predictions[45]. The majority of these I-band Ig domains (~80%) possess two or more evolutionarily conserved cryptic cysteines, which can potentially form disulfide bonds under oxidative stress. Since both sequence and structural-topological features are highly conserved[16,21,23,38,63], the sensitivity of the force-dependent unfolding rate to proline isomerization and disulfide bond formation is likely a shared characteristic of these I-band Ig domains. This has important implications for the structural states of the Ig domains and their interactions with binding factors.

Previous studies on titin I27 suggest that the I-band Ig domains exhibit high mechanical stability, with unfolding rates ranging from 10^{-3} s^{-1} to 10^{-4} s^{-1} within 30 pN[11,12]. This implies that the Ig domains have low structural dynamics during muscle contraction and extension. In contrast, the results presented here show that, even at room temperature, the majority of the Ig domains in the I-band exist in two mechanically distinct native states. The trans-Ig1 domains exhibit unfolding rates of approximately 1 s^{-1}, over 1000 times faster than the cis-Ig1 domains. These findings suggest that the titin I-band Ig domains may display much greater structural dynamics within the physiological force range. Such dynamic unfolding and refolding of the Ig domains may transiently expose binding sites for various factors, which could

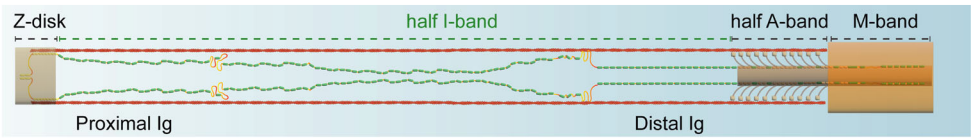

Region		Domain (Uniprot: Q8WZ42-1)	Cis-Pro containing domain count (AlphaFold prediction)		Cis-Pro structural position		N of Cys-containing domains (⩾2)
			N of domains	N of Cis-Pro	B-C loop	Other	
Z-disk		Ig-like 1-9	9 (100%)	10	9	1	5 (56%)
I-band	proximal	Ig-like 10-79	43 (61%)	43	42	1	59 (84%)
	distal	Ig-like 80-94	1 (7%)	1	1	0	9 (60%)
A&M-band		Ig-like 95-152	55 (95%)	56	55	1	16 (28%)
Total		Ig-like 1-152	108 (71%)	110	107	3	89 (59%)

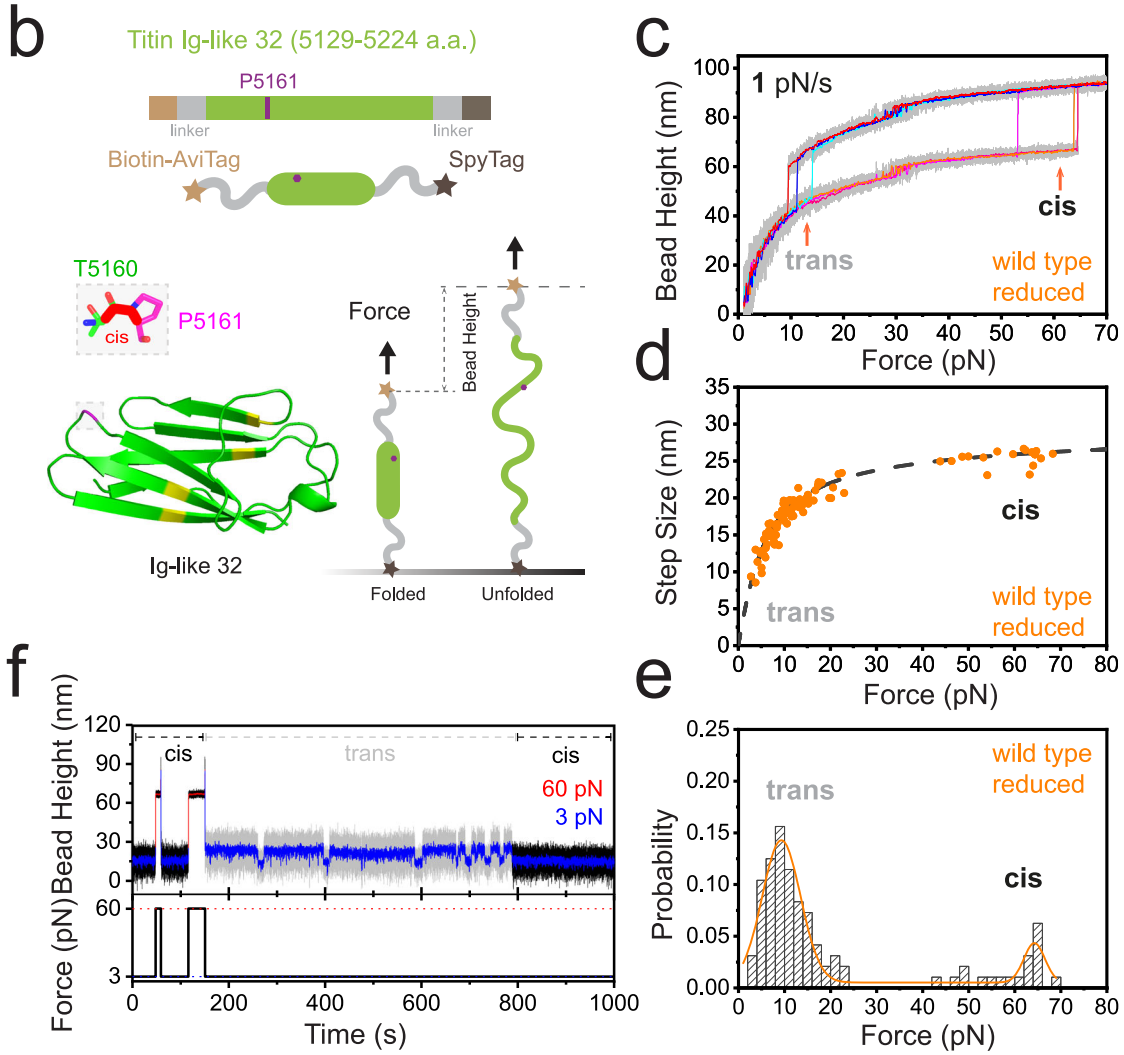

be critical for the mechanochemical functions and homeostasis of the titin I-band.

The mechanical stability of a protein domain is primarily determined by the interactions of residues along the unfolding transition pathway. For the titin Ig domain, which has a well-characterized seven β-strand structure, the 1st (A) and 7th (G) strands are in close proximity in a shearing-force stretching geometry[23]. The unfolding pathway of the titin Ig domain is thought to involve the sequential peeling of the 1st (A) strand from the folded core of the domain. While proline isomerization or point mutations (located in the loop bridging the 2nd (B) and 3rd (C) strands), as well as the disulfide bond (located between the 3rd (C) and 5th (E) strands), do not significantly alter the primary unfolding pathway, changes to the folded core may affect the effective energy barrier between the native and transition

Fig. 5 | Proline-isomerization mediated two mechanically distinct native states are conserved in titin I-band Ig domains. a The summary table of titin Ig domains with the number of domains containing cis-pro or cys residues. **b** Illustration of the single-molecule experiments designed for probing the titin Ig-like 32 mechanics. The structural sketch was predicted by AlphaFold3, and the Cis-proline (P5161) is highlighted in the zoom-in. **c** Representative force--bead height curves of the titin Ig-like 32 during linear force-increase scans with a loading rate of 1 pN s^{-1}. The raw data (gray) is 10-point FFT smoothed (colored lines). **d**, **e** The resulting force--step size distributions (**d**) and the normalized unfolding force distributions (**e**) of the Ig-like 32 unfolding events obtained from the linear force-loading scans. The number of data points for the statistics is $N = 96$, with a bin size of 2 pN. The dashed line in (**d**) is the theoretical calculation of the force-dependent step size of the Ig-like 32. The colored line in (**e**) is the double-Gaussian fitting of the distribution, giving the peak forces as 9.3 ± 4.1 pN and 64.3 ± 2.3 pN. **f** A representative time--bead height curve during force-jump cycles. The Ig-like 32 was initially maintained in the cis state at 3 pN, and then unfolded at 60 pN in the cis state, then rapidly refolded at 3 pN in the cis state. In the second cycle, the Ig-like 32 was unfolded at 60 pN in the cis state and then transited into the trans-state. When force was returned to 3 pN, the Ig-like 32 underwent dynamic refolding and unfolding fluctuations in the trans-state for over 600 s, until switched into cis state and rapidly refolded in stable cis state at 3 pN.

states. Consequently, this can lead to changes in the force-dependent unfolding rates.

In the transition state, the extension of the peeled A strand is force-dependent: it increases with rising force, following the worm-like chain model. At low forces, its extension is shorter than that of the A strand in the extended β-strand conformation within the folded domain, resulting in a negative transition distance. At higher forces, its extension surpasses that of the β-strand, causing the transition distance to become positive. This shift leads to slip-bond unfolding at high forces. Thus, the force-dependent extension change in the transition state drives the catch-slip transition of the Ig domains.

Interestingly, the formation of a disulfide bond in oxidized Ig1 promotes the emergence of a hidden intermediate state along the unfolding pathway. This hidden intermediate possibly involves the B-F strands located in the folded core. We speculate that this hidden intermediate state may also exist in reduced Ig1 but with a significantly lower energy barrier, which does not hinder the unfolding process within our measured force range. Conversely, in oxidized Ig1, the disulfide bond between the C-E strands stabilizes the folded core and increases the energy barrier of the hidden intermediate state. This elevated energy barrier accounts for the slip-bond behavior observed in oxidized Ig1 at low forces. Whether this hidden intermediate state is a general feature of titin Ig domains remains to be explored in future studies.

Consistently, a more stable folded core also facilitates the refolding process. The folded core containing the disulfide bond is more stable than the reduced folded core, resulting in a faster refolding rate for oxidized Ig1 compared to reduced Ig1 at the same force, in both the proline cis-state and trans-state (Supplementary Fig. 15). Furthermore, the proline cis-state folded core is more stable than the trans-state folded core, leading to a faster refolding rate for cis-state Ig1 relative to trans-state Ig1 at the same force (Supplementary Fig. 15).

The intrinsically slow proline isomerization and disulfide bond formation strongly affect the folding and unfolding dynamics of proteins, thereby they may act as a highly effective regulatory mechanism in a wide array of biological processes[26–32]. The proline isomerization and disulfide bond formation, in turn, are also modulated by the domains' folding or unfolding states. Mechanical forces are effective regulators of the structural states of protein domains. Since mechanosensitive proteins, such as titin and filamin, are physiologically regulated by mechanical forces, the interplay among mechanical forces, proline isomerization, and disulfide bond formation may serve as an important modulator for conformational changes and interactions, thereby influencing the functions of mechanosensitive proteins. The idea has been suggested in structural studies of the A2 domain of von Willebrand factor[64] and experimentally demonstrated with the first β-strand of domain 20 (FLNa20) of human filamin A using single-molecule optical tweezers[32]. Importantly, in both filamin and titin, based on the AlphaFold3 structural prediction, the majority of force-bearing domains contain cis-proline in their folded states, suggesting that this may be a general regulatory mechanism for such proteins.

We have previously demonstrated that the unfolding rate of the titin I27 domain is highly sensitive to temperature changes within the physiological range[14]. Over a force range up to 20 pN, an increase in temperature from 23 °C to 37 °C results in a two-order-of-magnitude increase in the unfolding rate (from 10^{-3} s^{-1} to 10^{-1} s^{-1}). Given the highly conserved sequences and structural features of titin Ig domains, Ig1 and other Ig domains may also exhibit strong sensitivity to temperature. We, therefore, hypothesize that under in vivo temperature conditions (37 °C), the majority of titin I-band Ig domains (specifically the cis-proline containing Ig domains) are predominantly unfolded when they transition from the cis-state to the trans-state under physiological forces due to the combined effects of temperature and proline isomerization. The remaining Ig domains likely undergo dynamic unfolding and refolding fluctuations as a result of temperature effects. This highly dynamic behavior of titin I-band Ig domains highlights their potential force-dependent signaling roles, as well as the importance of chaperone proteins. Further studies are needed to explore the effects of temperature on the force-dependent unfolding rates of Ig1 and other Ig domains, as well as the influence of chaperone proteins on these Ig domains.

Methods

Plasmids preparation and protein expression

Four plasmids were prepared for the expression of the protein constructs for single-molecule stretching experiments: (1) pET151-Avi-(Ig1)-Spy, (2) pET151-Avi-($Ig1^{P2105G}$)-Spy, (3) pET151-Avi-($Ig1^{P2105A}$)-Spy, (4) pET28a-Avi-(Ig-like 32)-Spy. The target genes were synthesized by IDTgblock/Sangon, assembled into pET151 or pET28a vectors using a seamless DNA assembly kit and verified by first-generation sequencing (Sangon). Detailed sequence information for the single-molecule protein constructs is provided in Supplementary Note 1.

Proteins were purified as previously described[49,65]. Briefly, each plasmid was transformed into BirA-containing *Escherichia coli* BL21 (DE3) by heat shock (42 °C for 40 s) and cultured overnight (≥ 12 h) on an LB agar plate at 37 °C. A single colony was picked and cultured in 5 mL of LB broth medium overnight (12–14 h) at 37 °C with shaking at 250 rpm. Next, 4 mL of the overnight culture was diluted into 400 mL of fresh LB broth medium (1:100 ratio) and incubated at 37 °C with shaking at 250 rpm for 2-3 h until the optical density (OD) reached 0.4-0.6. D-Biotin and IPTG were then added to final concentrations of 50 μM and 0.4 mM, respectively. The culture was incubated overnight (approximately 16 hours) at 20 °C with shaking at 250 rpm. Bacteria were harvested by centrifugation at 4000 rpm at room temperature and resuspended in bacterial lysis buffer containing 50 mM Tris (pH 7.5), 500 mM NaCl, 10% glycerol, and 20 mM imidazole. Lysis was performed via sonication, and the lysate supernatant was incubated with Ni-NTA resin for approximately 3 hours with gentle shaking at 4 °C. The protein was eluted using a buffer containing 50 mM Tris (pH 7.5), 500 mM NaCl, 10% glycerol, 1 mM β-Mercaptoethanol, and 200 mM imidazole. Imidazole was removed via buffer exchange using dialysis or the ÄKTA system. The final protein concentration was approximately 1 mg mL^{-1} in a storage buffer composed of 50 mM Tris (pH 7.5), 500 mM NaCl, 5 mM DTT (Dithiothreitol), and 10% glycerol.

Protein aliquots were snap-frozen in liquid nitrogen and stored at −80 °C.

AlphaFold based structural prediction

All 152 known human titin Ig-like domains (UniProt: Q8WZ42-1) were predicted using AlphaFold3 via the AlphaFold server (available at https://deepmind.google/technologies/alphafold/alphafold-server/). The predictions were generated between May 15, 2024, and May 25, 2024, with the exact prediction time for each domain recorded in the original files (available as source data files). Briefly, the amino acid sequence of each Ig-like domain, as annotated in UniProt (Q8WZ42-1), was uploaded to the server. The server produced five structural models (i.e., model-0, model-1, model-2, model-3, and model-4) along with associated parameters such as pLDDT and PAE, which were downloaded for analysis. In this study, we used model-0 for each domain in our analyses (Fig. 5a and Supplementary Figs. 4–11). The predicted models are subject to the AlphaFold Server Output Terms of Use (available at alphafoldserver.com/output-terms). No modifications were made to the original predictions, and all structures were used strictly for non-commercial, scientific research purposes.

Single-protein manipulation

All in vitro protein stretching experiments were performed using home-built vertical magnetic tweezers[46,47,50,65–67] in a reduced-state solution containing 1X PBS, 1% BSA, 2.5 mM DTT, and 10 mM sodium L-ascorbate, or in a solution that allows cysteine oxidation, consisting of 1X PBS and 1% BSA. The experiments were conducted at 22 ± 1 °C. The magnetic tweezers setup has a temporal resolution of 200 Hz and a spatial resolution of approximately 0.8 nm. Force calibration of the setup introduces a 5–10% uncertainty due to the heterogeneity in the diameter of the paramagnetic beads[46], while the determination of bead height in the setup has an uncertainty of approximately 2 nm due to the thermal fluctuation of the tethered bead[66]. Raw data from the magnetic tweezers experiments were analyzed using OriginPro or MATLAB software and plotted using OriginPro.

Theoretical calculation of transition step sizes

The force-extension curve of a folded domain, $x^{\text{rigid body}}(F)$, is determined by the rigid rotational fluctuations of a characteristic rigid body with a length of b, which can be estimated from the structure of the folded domain. This curve can be described using the freely-jointed chain polymer model with a single segment:

$$x^{\text{rigid body}}(F) = b\left(\coth\left(\frac{Fb}{k_B T}\right) - \frac{k_B T}{Fb}\right) \tag{5}$$

The force-extension curve of the unfolded state of a domain is determined by the force response of a flexible peptide chain. This curve can be described using the worm-like chain (WLC) polymer model with the Marko-Siggia formula[52]:

$$\frac{FA}{k_B T} = \frac{1}{4\left(1 - \frac{x^{\text{WLC}}(F)}{Nl_0}\right)^2} - \frac{1}{4} + \frac{x^{\text{WLC}}(F)}{Nl_0} \tag{6}$$

where A ~ 0.8 nm is the bending persistence length of the residues, l_0 = 0.38 nm is the contour length per residue[11,17,68], and N is the number of residues in the unfolded domain. Therefore, the force-dependent unfolding transition step size, defined as the change in extension of the domain before and after unfolding at the transition force, is given by:

$$\Delta x_{\text{UN}}(F) = x^{\text{WLC}}(F) - x^{\text{rigid body}}(F) \tag{7}$$

Ig1 domain contains approximately 95 amino acid residues and has a rigid body length of ~ 4.3 nm. In the reduced state, all residues are released upon unfolding. In the oxidized state, where two cysteine residues form a disulfide bond, 24 residues are locked within the disulfide bond, leading to 71 residues for releasing upon domain unfolding. Based on these estimates and the above equations, we can calculate the theoretical force-dependent unfolding or refolding transition step sizes of Ig domains in both reduced and oxidized states.

Arrhenius Law analysis of force-dependent refolding rates

The refolding rates of Ig1 can be described by Arrhenius Law:

$$k_r(F) = k_r^0 \exp\left(-\frac{\Delta G^*(F)}{k_B T}\right) \tag{8}$$

where k_r^0 is the zero-force refolding rate and $\Delta G^*(F) = -\int_0^F \Delta x^*(f) df$, represents the free energy difference between the transition state and the unfolded state. Here, $\Delta x^*(f) = x^*(f) - x_{\text{unfolded}}(f)$ is the force-dependent transition distance. By treating the transition state as a rigid body with a length b^* and the unfolded state as a flexible peptide, $x^*(f)$ could be then described by the freely-jointed chain model, and $x_{\text{unfolded}}(f)$ could be described by the WLC model using Marko-Siggia formula[52]. All fitting parameters are summarized in Supplementary Table 4.

Apparent proline isomerization rate analysis

There are a total of four states for either reduced or oxidized Ig1, U_{trans}, U_{cis}, N_{trans}, and N_{cis} (Fig. 4a). The apparent proline isomerization rate, $k_{t\text{-}c}^{\text{app}}(F)$, measures the transition rate from U_{trans} to N_{cis} (Fig. 4b–d). Before reaching N_{cis}, the domain can be in U_{trans}, U_{cis}, or N_{trans} state. The probability of being in the U_{trans} state is given by $P_{U,t}(F) = k_u^{\text{trans}}(F)/[k_u^{\text{trans}}(F) + k_r^{\text{trans}}(F)]$, while the probability of being in the N_{trans} state is $1 - P_{U,t}(F)$. In both states, proline can undergo isomerization, resulting in two distinct pathways originating from two different starting points (U_{trans} and N_{trans}). For the pathway starting from U_{trans}, the isomerization proceeds through U_{cis} and ends at N_{cis}, allowing the U_{cis} state can be treated as an intermediate state. Consequently, the net transition rate of the U_{trans}-U_{cis}-N_{cis} path can be expressed as a combination of $k_{t\text{-}c}^{U}$, k_r^{cis} and $k_{c\text{-}t}^{U}$[60]. For the pathway of U_{trans}-N_{trans}-N_{cis}, the isomerization rate is denoted as $k_{t\text{-}c}^{N}$. Combining the rates of these two pathways with the probabilities of originating from their respective start points gives Eq. (1).

Reporting summary

Further information on research design is available in the Nature Portfolio Reporting Summary linked to this article.

Data availability

Unless otherwise stated, all data supporting the results of this study can be found in the article, Supplementary, and source data files. Sequence information of key constructs is included in Supplementary Information. AlphaFold-predicted structures are available as source data files. The predicted models are subject to the AlphaFold Server Output Terms of Use (available at alphafoldserver.com/output-terms). No modifications were made to the original predictions, and all structures were used strictly for non-commercial, scientific research purposes. Key plasmids are available upon request from the corresponding authors. Source data are provided in this paper.

References

1. Grison, M., Merkel, U., Kostan, J., Djinović-Carugo, K. & Rief, M. α-actinin/titin interaction: A dynamic and mechanically stable cluster of bonds in the muscle Z-disk. *Proc. Natl. Acad. Sci. USA* **114**, 1015–1020 (2017).
2. Bertz, M., Wilmanns, M. & Rief, M. The titin-telethonin complex is a directed, superstable molecular bond in the muscle Z-disk. *Proc. Natl. Acad. Sci. USA* **106**, 13307–133310 (2009).

3. Labeit, S., Kolmerer, B. & Linke, W. A. The giant protein titin. emerging roles in physiology and pathophysiology. *Circ. Res.* **80**, 290–4 (1997).
4. Linke, W. A., Ivemeyer, M., Mundel, P., Stockmeier, M. R. & Kolmerer, B. Nature of PEVK-titin elasticity in skeletal muscle. *Proc. Natl. Acad. Sci. USA* **95**, 8052–7 (1998).
5. Linke, W. A. et al. Towards a molecular understanding of the elasticity of titin. *J. Mol. Biol.* **261**, 62–71 (1996).
6. Cazorla, O. et al. Differential expression of cardiac titin isoforms and modulation of cellular stiffness. *Circ. Res.* **86**, 59–67 (2000).
7. Linke, W. A. & Granzier, H. A spring tale: New facts on titin elasticity. *Biophys. J.* **75**, 2613–2614 (1998).
8. Linke, W. A., Stockmeier, M. R., Ivemeyer, M., Hosser, H. & Mundel, P. Characterizing titin's I-band Ig domain region as an entropic spring. *J. Cell Sci.* **111**, 1567–1574 (1998).
9. Freundt, J. K. & Linke, W. A. Titin as a force-generating muscle protein under regulatory control. *J. Appl. Physiol.* **126**, 1474–1482 (2019).
10. Pang, S. M., Le, S. & Yan, J. Mechanical responses of the mechanosensitive unstructured domains in cardiac titin. *Biol. Cell* **110**, 65–76 (2018).
11. Chen, H. et al. Dynamics of equilibrium folding and unfolding transitions of titin immunoglobulin domain under constant forces. *J. Am. Chem. Soc.* **137**, 3540–6 (2015).
12. Yuan, G. et al. Elasticity of the transition state leading to an unexpected mechanical stabilization of titin immunoglobulin domains. *Angew. Chem. Int. Ed.* **56**, 5490–5493 (2017).
13. Rivas-Pardo, J. A. et al. Work done by titin protein folding assists muscle contraction. *Cell Rep.* **14**, 1339–1347 (2016).
14. Yu, M., Lu, J.-H., Le, S. & Yan, J. Unexpected low mechanical stability of titin I27 domain at physiologically relevant temperature. *J. Phys. Chem. Lett.* **12**, 7914–7920 (2021).
15. Politou, A. S., Thomas, D. J. & Pastore, A. The folding and stability of titin immunoglobulin-like modules, with implications for the mechanism of elasticity. *Biophys. J.* **69**, 2601–10 (1995).
16. Improta, S., Politou, A. S. & Pastore, A. Immunoglobulin-like modules from titin I-band: extensible components of muscle elasticity. *Structure* **4**, 323–37 (1996).
17. Rief, M., Gautel, M., Oesterhelt, F., Fernandez, J. M. & Gaub, H. E. Reversible unfolding of individual titin immunoglobulin domains by AFM. *Science* **276**, 1109–12 (1997).
18. Best, R. B. et al. Mechanical unfolding of a titin Ig domain: structure of transition state revealed by combining atomic force microscopy, protein engineering and molecular dynamics simulations. *J. Mol. Biol.* **330**, 867–77 (2003).
19. Botello, E. et al. Temperature and chemical denaturant dependence of forced unfolding of titin I27. *J. Phys. Chem. B* **113**, 10845–8 (2009).
20. Yagawa, K. et al. Structural basis for unfolding pathway-dependent stability of proteins: vectorial unfolding versus global unfolding. *Protein Sci.* **19**, 693–702 (2010).
21. Fowler, S. B. & Clarke, J. Mapping the folding pathway of an immunoglobulin domain: structural detail from phi value analysis and movement of the transition state. *Structure* **9**, 355–66 (2001).
22. Stacklies, W., Vega, M. C., Wilmanns, M. & Gräter, F. Mechanical network in titin immunoglobulin from force distribution analysis. *PLoS Comput. Biol.* **5**, e1000306 (2009).
23. Marino, M. et al. Poly-Ig tandems from I-band titin share extended domain arrangements irrespective of the distinct features of their modular constituents. *J. Muscle Res. Cell Motility* **26**, 355–65 (2005).
24. Alegre-Cebollada, J. et al. S-glutathionylation of cryptic cysteines enhances titin elasticity by blocking protein folding. *Cell* **156**, 1235–1246 (2014).
25. Beckendorf, L. & Linke, W. A. Emerging importance of oxidative stress in regulating striated muscle elasticity. *J. Muscle Res. Cell Motility* **36**, 25–36 (2015).
26. Lummis, S. C. R. et al. Cis-trans isomerization at a proline opens the pore of a neurotransmitter-gated ion channel. *Nature* **438**, 248–252 (2005).
27. Eckert, B., Martin, A., Balbach, J. & Schmid, F. X. Prolyl isomerization as a molecular timer in phage infection. *Nat. Struct. Mol. Biol.* **12**, 619–623 (2005).
28. Charbonnier, J., Belin, P., Moutiez, M., Stura, E. A. & Quéméneur, E. On the role of the cis-proline residue in the active site of DsbA. *Protein Sci.* **8**, 96–105 (1999).
29. Jakob, R. P. & Schmid, F. X. Energetic coupling between native-state prolyl isomerization and conformational protein folding. *J. Mol. Biol.* **377**, 1560–1575 (2008).
30. Sarkar, P., Reichman, C., Saleh, T., Birge, R. B. & Kalodimos, C. G. Proline cis-trans isomerization controls autoinhibition of a signaling protein. *Mol. Cell* **25**, 413–426 (2007).
31. Lu, K. P., Finn, G., Lee, T. H. & Nicholson, L. K. Prolyl cis-trans isomerization as a molecular timer. *Nat. Chem. Biol.* **3**, 619–629 (2007).
32. Rognoni, L., Möst, T., Žoldák, G. & Rief, M. Force-dependent isomerization kinetics of a highly conserved proline switch modulates the mechanosensing region of filamin. *Proc. Natl. Acad. Sci. USA* **111**, 5568–5573 (2014).
33. Wedemeyer, W. J., Welker, E. & Scheraga, H. A. Proline cis–trans isomerization and protein folding. *Biochemistry* **41**, 14637–14644 (2002).
34. Brandts, J. F., Halvorson, H. R. & Brennan, M. Consideration of the possibility that the slow step in protein denaturation reactions is due to cis-trans isomerism of proline residues. *Biochemistry* **14**, 4953–4963 (1975).
35. Brandts, J. F., Brennan, M. & Lin, L.-N. Unfolding and refolding occur much faster for a proline-free proteins than for most proline-containing proteins. *Proc. Natl. Acad. Sci. USA* **74**, 4178–4181 (1977).
36. Kiefhaber, T., Grunert, H. P., Hahn, U. & Schmid, F. X. Replacement of a cis proline simplifies the mechanism of ribonuclease T1 folding. *Biochemistry* **29**, 6475–6480 (1990).
37. Pappenberger, G. et al. Kinetic mechanism and catalysis of a native-state prolyl isomerization reaction. *J. Mol. Biol.* **326**, 235–246 (2003).
38. Mayans, O., Wuerges, J., Canela, S., Gautel, M. & Wilmanns, M. Structural evidence for a possible role of reversible disulphide bridge formation in the elasticity of the muscle protein titin. *Structure* **9**, 331–340 (2001).
39. Pfuhl, M., Improta, S., Politou, A. & Pastore, A. When a module is also a domain: the role of the N terminus in the stability and the dynamics of immunoglobulin domains from titin. *J. Mol. Biol.* **265**, 242–256 (1997).
40. Marino, M. et al. The Ig doublet Z1Z2: A model system for the hybrid analysis of conformational dynamics in ig tandems from titin. *Structure* **14**, 1437–1447 (2006).
41. Chatziefthimiou, S. D. et al. Structural diversity in the atomic resolution 3D fingerprint of the titin M-band segment. *PLOS ONE* **14**, e0226693 (2019).
42. Stronczek, C. et al. The N2A region of titin has a unique structural configuration. *J. Gen. Physiol.* **153**, e202012766 (2021).
43. Martinez-Martin, I. et al. Titin domains with reduced core hydrophobicity cause dilated cardiomyopathy. *Cell Rep.* **42**, 113490 (2023).
44. Kelly, C. & Gage, M. J. Protein unfolding: Denaturant vs. force. *Biomedicines* **9**, 1395 (2021).
45. Jumper, J. et al. Highly accurate protein structure prediction with alphafold. *Nature* **596**, 583–589 (2021).

46. Chen, H. et al. Improved high-force magnetic tweezers for stretching and refolding of proteins and short DNA. *Biophys. J.* **100**, 517–523 (2011).
47. Le, S., Liu, R., Lim, C. T. & Yan, J. Uncovering mechanosensing mechanisms at the single protein level using magnetic tweezers. *Methods* **94**, 13–18 (2016).
48. Zakeri, B. et al. Peptide tag forming a rapid covalent bond to a protein, through engineering a bacterial adhesin. *Proc. Natl. Acad. Sci. USA* **109**, E690–7 (2012).
49. Le, S. et al. Mechanotransmission and mechanosensing of human alpha-actinin 1. *Cell Rep.* **21**, 2714–2723 (2017).
50. Le, S. et al. Disturbance-free rapid solution exchange for magnetic tweezers single-molecule studies. *Nucleic Acids Res.* **43**, e113–e113 (2015).
51. Guo, Z. et al. Spytag/spycatcher tether as a fingerprint and force marker in single-molecule force spectroscopy experiments. *Nanoscale* **13**, 11262–11269 (2021).
52. Marko, J. F. & Siggia, E. D. Stretching DNA. *Macromolecules* **28**, 8759–8770 (1995).
53. Guo, S. et al. Structural-elastic determination of the force-dependent transition rate of biomolecules. *Chem. Sci.* **9**, 5871–5882 (2018).
54. Huang, W. et al. Mechanical stabilization of a bacterial adhesion complex. *J. Am. Chem. Soc.* **144**, 16808–16818 (2022).
55. Marszalek, P. E. et al. Mechanical unfolding intermediates in titin modules. *Nature* **402**, 100–3 (1999).
56. Williams, P. M. et al. Hidden complexity in the mechanical properties of titin. *Nature* **422**, 446–9 (2003).
57. Gao, M., Wilmanns, M. & Schulten, K. Steered molecular dynamics studies of titin I1 domain unfolding. *Biophys. J.* **83**, 3435–45 (2002).
58. Pierse, C. A. & Dudko, O. K. Distinguishing signatures of multi-pathway conformational transitions. *Phys. Rev. Lett.* **118**, 088101 (2017).
59. Guo, Z. et al. Hidden intermediate state and second pathway determining folding and unfolding dynamics of GB1 protein at low forces. *Phys. Rev. Lett.* **125**, 198101 (2020).
60. Garai, A., Zhang, Y. & Dudko, O. K. Conformational dynamics through an intermediate. *J Chem Phys.* **140**, 135101 (2014).
61. Bell, G. I. Models for the specific adhesion of cells to cells: A theoretical framework for adhesion mediated by reversible bonds between cell surface molecules. *Science* **200**, 618–627 (1978).
62. Urbanek, A. et al. Evidence of the reduced abundance of proline cis conformation in protein poly proline tracts. *J. Am. Chem. Soc.* **142**, 7976–7986 (2020).
63. Clarke, J., Cota, E., Fowler, S. B. & Hamill, S. J. Folding studies of immunoglobulin-like beta-sandwich proteins suggest that they share a common folding pathway. *Structure* **7**, 1145–53 (1999).
64. Zhang, Q. et al. Structural specializations of A2, a force-sensing domain in the ultralarge vascular protein von willebrand factor. *Proc. Nat. Acad. Sci. USA* **106**, 9226–9231 (2009).
65. Zhang, Y. et al. Multi-domain interaction mediated strength-building in human α-actinin dimers unveiled by direct single-molecule quantification. *Nat. Commun.* **15**, 6151 (2024).
66. Le, S., Yu, M. & Yan, J. Direct single-molecule quantification reveals unexpectedly high mechanical stability of vinculin-talin–alpha-catenin linkages. *Sci. Adv.* **5**, eaav2720 (2019).
67. Le, S., Yu, M. & Yan, J. Phosphorylation reduces the mechanical stability of the α-catenin/ β-catenin complex. *Angew. Chem. Int. Ed.* **58**, 18663–18669 (2019).
68. Le, S., Yu, M. & Yan, J. Mechanical regulation of tension-transmission supramolecular linkages. *Curr. Opin. Solid State Mater. Sci.* **25**, 100895 (2021).

Acknowledgements

The research is funded by the National Natural Science Foundation of China (NSFC Grant NO.32301094 and 12474202 to M.Y., NO. 12204389 and 32271367 to S.L., NO.12474200 to H.C.) and the 111 Project (B16029). J.Y. acknowledges the support from the Undergraduate Innovation Program of Xiamen University. The authors acknowledge the insightful discussions with Prof. Jie Yan (National University of Singapore), Prof. Chenxu Wu (Xiamen University) and Prof. Wei Chen (Zhejiang University). The authors would like to extend their sincere gratitude to all the reviewers for their insightful comments and constructive suggestions.

Author contributions

S.L. and M.Y. conceived the study; S.L., M.Y., H.C., and Y.W. designed the experiments; Y.W. performed the single-molecule experiments; J.Y., F.S., Y.Z., X.Q., J.X., X.L., J.D., Z.Z., and H.S. provided technological support; S.L., M.Y., H.C., Y.W., and J.Y. analyzed and interpreted the data; S.L. and M.Y. wrote the paper with inputs from all authors.

Competing interests

The authors declare no competing interests.

Additional information

Supplementary information The online version contains supplementary material available at https://doi.org/10.1038/s41467-025-57989-y.

Correspondence and requests for materials should be addressed to Hu Chen, Miao Yu or Shimin Le.

Peer review information *Nature Communications* thanks Stefano Giordano, Mark Pfuhl, and the other anonymous reviewer(s) for their contribution to the peer review of this work. A peer review file is available.

Reprints and permissions information is available at http://www.nature.com/reprints

Publisher's note Springer Nature remains neutral with regard to jurisdictional claims in published maps and institutional affiliations.

Open Access This article is licensed under a Creative Commons Attribution-NonCommercial-NoDerivatives 4.0 International License, which permits any non-commercial use, sharing, distribution and reproduction in any medium or format, as long as you give appropriate credit to the original author(s) and the source, provide a link to the Creative Commons licence, and indicate if you modified the licensed material. You do not have permission under this licence to share adapted material derived from this article or parts of it. The images or other third party material in this article are included in the article's Creative Commons licence, unless indicated otherwise in a credit line to the material. If material is not included in the article's Creative Commons licence and your intended use is not permitted by statutory regulation or exceeds the permitted use, you will need to obtain permission directly from the copyright holder. To view a copy of this licence, visit http://creativecommons.org/licenses/by-nc-nd/4.0/.

© The Author(s) 2025